Tunable Magnetism in Strained Graphene with Topological Line Defect

Liangzhi Kou,[†,‡,§,*] Chun Tang,[†,§] Wanlin Guo,[‡,*] and Changfeng Chen[†,*]

[†]Department of Physics and High Pressure Science and Engineering Center, University of Nevada, Las Vegas, Nevada 89154, United States, and [‡]Institute of Nano Science, Nanjing University of Aeronautics and Astronautics, Nanjing 210016, China. [§] These authors contributed equally to this work.

ABSTRACT We examine the magnetic properties of two-dimensional graphene with topological line defect using first-principles calculations and predict a weak ferromagnetic ground state with spin-polarized electrons localized along the extended line defect. Our results show that tensile strain along the zigzag direction can greatly enhance local magnetic moments and ferromagnetic stability of the system. In sharp contrast, tensile strain applied along the armchair direction quickly diminishes these magnetic moments. A detailed analysis reveals that this intriguing magnetism modulation by strain stems from the redistribution of spin-polarized electrons induced by local lattice distortion. It suggests a sensitive and effective way to control magnetic properties of graphene which is critical for its applications in nanoscale devices.

KEYWORDS: graphene · topological line defect · magnetism modulation · strain control

Graphene, a single graphite layer, is emerging as an extremely versatile material with outstanding properties suitable for spintronics and nanodevice applications.[1−3] Nevertheless, such proposed applications of graphene require the ability to tune its electronic or magnetic properties at the nanoscale.[4,5] Although charge transfer and field-effect doping can be applied to manipulate charge carrier concentrations, how to achieve nanoscale control remains a challenge.[6,7] One of the alternative approaches is to introduce extended defects into the graphene lattice.[8] These defects are often characterized by pentagonal and heptagonal rings in the hexagonal carbon lattice and can be introduced by irradiation to alter their properties for suitable applications.[9−11] In particular, ferromagnetic ordering has been shown to exist among various defect configurations in graphene structures, such as vacancies, topological defects, edges, and hydrogen chemisorption.[12−16] To this end, a new type of one-dimensional topological defect in graphene, containing octagonal and pentagonal sp^2-hybridized carbon rings embedded in a perfect graphene sheet, has recently been produced experimentally. This new line defect structure is found to be a metallic wire and may play important roles in device application.[17] Theoretical calculations based on density functional theory have revealed intriguing electronic and magnetic properties of graphene and carbon nanotubes containing one-dimensional defect structures.[18−20] The controlled engineering of these defects represents a viable approach to creating and nanoscale controlling of one-dimensional charge distribution within widths of only several atoms.

A topic of considerable recent interest is the study of the interplay between the mechanical properties of graphene and its electronic/magnetic structure. The motivation for these studies is the possibility of tailoring the transport properties of graphene by means of externally induced strain. In previous studies, several groups have shown that the electronic spectrum of graphene can be strongly modified by external strain.[21−23] In particular, a strain over 20% in graphene might eventually lead to the opening of a band gap.[24] The effects of external strain on magnetic properties localized on the edge of zigzag graphene nanoribbons also have been explored.[25−27] These studies suggest the potential of strain as a way for tuning the electronic and magnetic properties of graphene.

In the present work, we employ first-principles calculations based on density functional theory to elucidate the effects of strain on magnetic properties of graphene with topological line defect. Similar to carbon nanotubes with such a line defect, the ground state of the defective graphene is ferromagnetic with small magnetic moments; the polarized electron spins are localized around the defect sites and ferromagnetically aligned along the extended line defect. We first examine the electronic and magnetic properties of the defective graphene in equilibrium, but our primary objective is to explore the effect of external strain on the magnetic properties

*Address correspondence to kouliangzhi@nuaa.edu.cn, wlguo@nuaa.edu.cn, chen@physics.unlv.edu.

Received for review September 15, 2010 and accepted January 5, 2011.

Published online January 13, 2011
10.1021/nn1024175

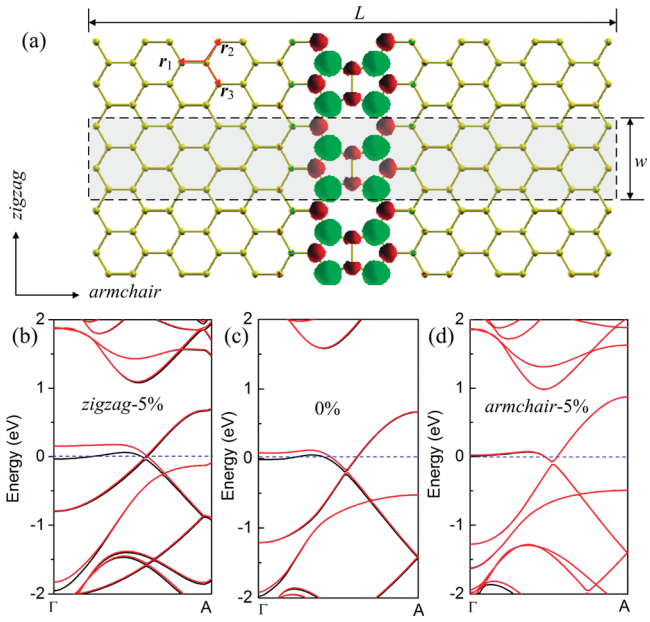

Figure 1. (a) Schematic illustration of the structural model of the relaxed two-dimensional graphene with an extended topological line defect. The shaded area covered by the dashed rectangle is the unit supercell (L = 2.977 nm) used in the present calculations. The spatial spin density distribution ($\rho_\downarrow - \rho_\uparrow$) is also plotted (spin-up, green; spin-down, red this color identification scheme is also used in other figures below). The value of the isosurface is 1×10^{-4} e/Å^3. The spin-polarized band structures of the graphene sheet with topological line defect (spin-up, black; spin-down, red) are shown for (b) 5% tensile strain along the zigzag direction, (c) 0% strain, and (d) 5% tensile strain along the armchair direction. Because the magnetism is originated from the spin splitting of the flat band near the Fermi level, only the band structures from Γ to A are presented.

of the system. We find that tensile strain along the zigzag direction of graphene greatly increases the electron localization, leading to the enhancement of the stability of the ferromagnetic state and the magnetic moments along the line defect over a large range of strain. However, further increase of strain results in a sharp reduction of the magnetic moments and the stability of the magnetic state. This effective modulation of magnetism occurs within the range of the elastic limit of graphene and, therefore, is fully reversible. In sharp contrast, tensile strain along the armchair direction produces the opposite effect (*i.e.*, diminishing the magnetic moments). Such sensitive modulation for magnetism holds great promise for applications of the graphene systems in nanoscale devices, especially those related to spintronics.

RESULTS AND DISCUSSION

Graphene with a topological line defect is metallic with a flat band crossing the Fermi level according to non-spin-polarized calculations.[17] Previous studies[12−16] show that such defects are closely associated with magnetism. Our calculations demonstrate that, when the spin polarization of atomic orbits is included in the calculations, a ferromagnetic ground state is always obtained after the self-consistent computation. This is the case even when an initial antiferromagnetic arrangement is chosen as the starting point. The spatial spin density distribution ($\rho_\downarrow - \rho_\uparrow$) of a fully relaxed graphene structure is shown in Figure 1a. It is seen that the spin-polarized electrons are localized in the region of the line defect, clearly exhibiting a ferromagnetic spin-ordering state. It decays rapidly with increasing distance away from the line defect. The spin-polarized band structure is also presented in Figure 1c. It shows a spin splitting flat band near the Fermi level, which loses its flatness at about $k = \pi/2$ and exhibits a substantial dispersion around the zone boundary. The flat band results from a delicate balance of electron transfers among the π orbitals situated near the topological line defect. From the structural character and spin-polarized electron distribution, the structure of graphene with topological line defect can be regarded as a combination of two zigzag graphene ribbons "glued" together by an array of C_2 at their zigzag edge sites. Therefore, the origin of the flat band states of graphene with line defect can be understood as a result of the edge states of the zigzag graphene nanoribbons.[18] Since the localized spin polarization in the line defect region may be affected by the neighboring line defect, it is necessary to investigate the effect of the length L between two adjacent line defects. We have examined three structural models with L = 1.414, 2.267, and 2.977 nm. The calculated magnetic moments are 0.14, 0.028, and 0.030 μ_B respectively. These results indicate that the magnetism is no longer affected by the adjacent line defect when the supercell length L in the armchair direction is larger than 2.267 nm. We therefore will focus our discussions below on the model with L = 2.267 nm.

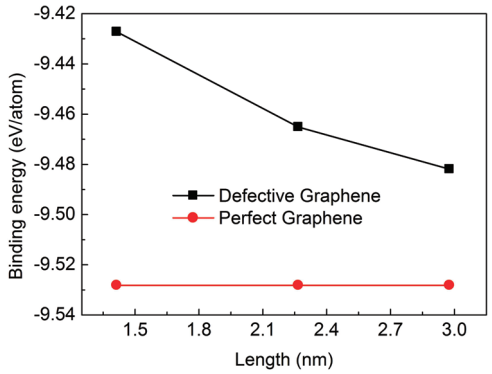

Figure 2. Binding energy per atom of the graphene with topological line defect as a function of the supercell length compared to that of perfect graphene.

In order to clarify the stability of the graphene with a topological line defect, we have investigated the binding energies and compared with those for defect-free graphene. Here the binding energy is defined as $E_b = (E_{tot} - nE_C)/n$, where E_{tot} and E_C are the total energy of the investigated system and that of a C atom, respectively; n is the number of C atoms. Figure 2 shows the results for the defective graphene as a function of supercell length L together with those of perfect graphene. It is seen that the binding energy of the graphene with a topological line defect is not much higher than that of perfect graphene and monotonically decreases with increasing supercell length. The binding energy of the defective graphene with $L = 2.977$ nm is only slightly higher (by 46.3 meV/atom) than that of the perfect graphene. These results indicate that the energy cost of introducing topological line defect to graphene is insignificant and, in particular, is unlikely to cause any problems for the structural integrity of the defective graphene.

We now examine the effect of strain on the magnetic properties. Due to the Poisson effect, stretching in one direction of the graphene will lead to contraction in the perpendicular direction; hence, in this study, the uniaxial strain is applied as follows:

$$\boldsymbol{\varepsilon} = \begin{pmatrix} \varepsilon & 0 \\ 0 & -\nu\varepsilon \end{pmatrix}$$

where ν is the Poisson ratio of graphene and ε is tensile strain. Following the results of previous work,[21] we take $\nu = 0.165$. As shown in Figure 3a, tensile strain along the zigzag direction has a significant effect on the magnetic properties. The magnetic moment exhibits a nearly linear relationship with increasing tensile strain at the early stage. As the strain increases to around 4%, the increase of the magnetic moment levels off before rising again with further increasing strain. After reaching a critical strain of about 12% (for $L = 2.267$ nm), further stretching leads to a sharp decline of the magnetic moment. Similar behavior of magnetism modulation is also observed in other models that we have considered (see, for example, the results for the structure with $L = 1.414$ nm also shown in Figure 3).

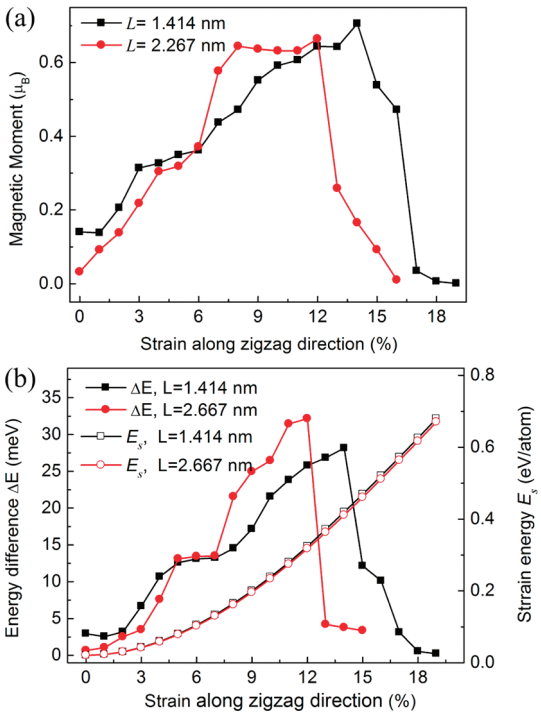

Figure 3. (a) Magnetic moment and (b) corresponding ferromagnetic stability (solid line) and strain energy (hollow line) as a function of applied strain along the zigzag direction.

Our calculations show that the ferromagnetic ground state in graphene with a topological line defect is not very stable (only a few millielectronvolts lower than the nonmagnetic state at zero strain). It is similar to the situation in armchair carbon nanotubes with a topological line defect.[13] This makes it impractical to use such graphene structures for device applications operating at room temperature conditions. To obtain robust magnetism suitable for applications, it is necessary to achieve a more stable magnetic state in the graphene system. Our calculations indicate that tensile strain along the zigzag direction provides a very effective solution: it enhances both the stability of the magnetic state and the magnetic moment of the defective graphene. The energy difference, defined as $\Delta E = E_{Nonmag} - E_{Ferro\text{-}mag}$, as a function of applied strain is presented in Figure 3b (solid line), where E_{Nonmag} and $E_{Ferro\text{-}mag}$ are the total energies of nonmagnetic and ferromagnetic states, respectively. It is interesting to see that the energy difference displays a very similar behavior to the magnetic modulation in response to applied strain along the zigzag direction. The maximum energy difference reaches 32.5 meV, which represents a more than 10-fold increase compared to the value for the unstrained state. It is noted that, while the sharp changes of the energy difference and the magnetic moment occur at the same critical strain, the value of the critical strain decreases with increasing L. For example, the critical strain is 14% for $L = 1.414$ nm

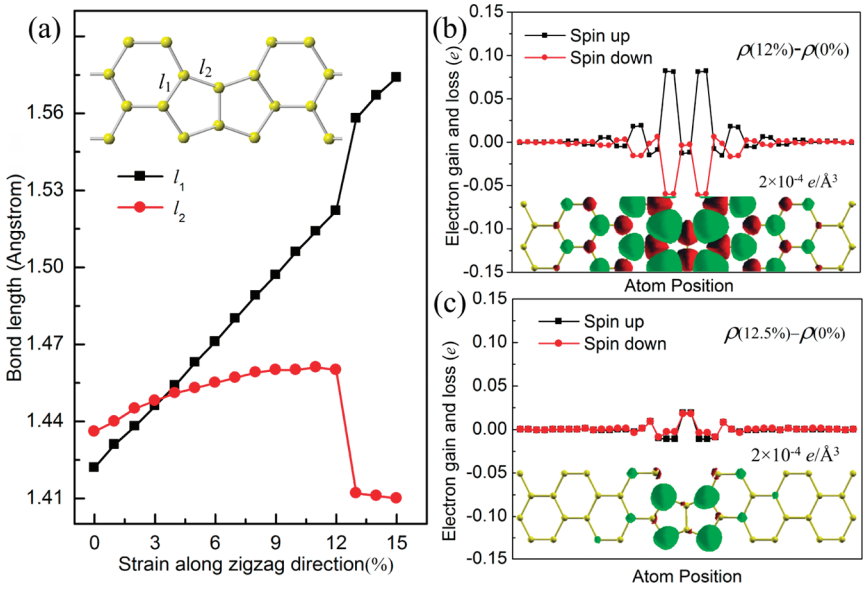

Figure 4. (a) Local bond length variation around the line defect region where the magnetism is localized. Definitions of l_1 and l_2 are given in the inset. The right panels show the spin density redistribution induced by applied strain: (b) ρ(12%) − ρ(0%) and (c) ρ(12.5%) − ρ(0%). Insets in (b) and (c) present the spin density contour plots in the corresponding strain state.

but reduces to 12% for L = 2.267 nm. Interestingly, although the magnetic behavior undergoes a sharp variation at the critical strain, it is not associated with a structural breakage or phase transition. As shown in Figure 3b, the strain energy increases as a quadratic function of strain even after the magnetic moments have diminished. This indicates that the magnetic modulation occurs within the elastic range and, therefore, is fully reversible. This feature is significant for practical nanomechanical control of the magnetic properties of the graphene system in device applications.

The enhancement of spin polarization under strain can be explained by an analytical model proposed by Fujita *et al.*[25] For localized states along a line defect, the corresponding charge density is proportional to 2 $\cos(k/2)^{2m}$ at each site of the mth zigzag chain away from the C_2 array. The factor 2 $\cos(k/2)$ represents a "damping length" of the localized states. When strain is applied, due to the distortions of the bond vector and the bond parameter, this damping factor is modified[21] to $2t_2/t_1 \cos(k/2)$, where t_1 and t_2 are bond parameters related to the bond vectors r_1 and r_2 shown in Figure 1a. For tensile strain along the zigzag direction, $|t_2/t_1| < 1$, the damping of localized states becomes much quicker, which results in more localized states along the line defect. Due to the electron−electron interaction, this will lead to a larger spin splitting of the band states near the Fermi level (Figure 1b), thus increasing the spin polarization in the region of the line defect. This picture is supported by our calculated spin density difference between strained and unstrained conditions, as shown in Figure 4b. In contrast, when a tensile strain is applied along the armchair direction, $|t_2/t_1| > 1$, and the damping of the localized states becomes much slower, resulting in the delocalization of such states with reduced electron correlation. Consequently, the band states near the Fermi level are non-spin-polarized, as shown in Figure 1d.

The above analytical model provides an explanation for the variation of magnetism under applied tensile strain along the zigzag or armchair direction when the graphene is considered as a combination of two (semi-infinite) zigzag nanoribbons. Meanwhile, it is noted that there is a sharp drop in magnetic moment at larger tensile strains along the zigzag direction. It is closely related to the variation of the local bond length at the defect sites where the spin-polarized electrons are localized. We explore this mechanism by examining the variation of the bond lengths near the defect line in response to applied strain. We focus on the response of two key bonds in the structure, as shown in Figure 4. It is seen that, before the strain reaches the critical value of about 12%, both bond lengths l_1 and l_2 increase monotonically with strain, which, according to the above-mentioned model studies,[18,19] would lead to increased electron localization and splitting of the states with opposite spin. This analysis is consistent with our calculated results that show a clear increase of spin-up state and decrease of spin-down state localized on the "zigzag edge atoms". It enhances the spin polarization along the line defect (see Figure 4b for spin density change at 12% strain compared to the results of the unstrained system). It is interesting to note that when strain reaches about 4% the two bond lengths intersect. This explains the appearance of a plateau in the plot of magnetic moment around 4% strain (see Figure 3a): it can be attributed to a delicate balance and competing nature of electron (de)localization and transfer resulting from the variations of these two bond lengths under the applied strain.

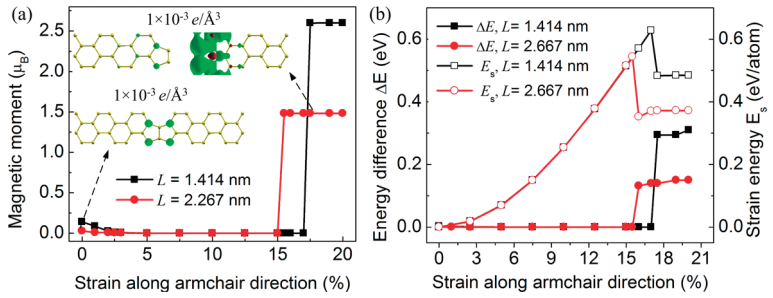

Figure 5. (a) Magnetic moment and (b) corresponding ferromagnetic stability (solid line) and strain energy (hollow line) as a function of applied strain along armchair direction. Insets in (a) show spin-polarized electron distributions under unstrained and strained conditions as indicated by dashed arrows.

Interestingly, when the strain exceeds 12%, the two bond lengths experience an abrupt change: l_1 suddenly increases while l_2 sharply decreases. By examining the spin-polarized electron transfer at 12.5% (Figure 4c) and comparing with those at 12% strain (Figure 4b), we find that such sudden variations of bond lengths induce significant redistribution of spin-polarized electrons, resulting in much less transfer of spin-polarized electrons to the "zigzag edge atoms" at 12.5% strain, as a consequence the electron delocalization induced by the sharp reduction of l_2. This leads to the decreased spin splitting and diminishing magnetic moments.

For a more comprehensive picture of strain effect, we also studied the magnetic modulation by tensile strain along the armchair direction. Contrary to the results by tensile strain along the zigzag direction, the weak magnetism in the unstrained structure quickly diminishes by the applied strain. It is caused by the electron delocalization due to the bond length change as discussed above and the accompanying reduction in spin polarization in the line defect region, resulting in a nonmagnetic state. The system remains in this nonmagnetic state until a structural breakage occurs at larger strains (see Figure 5a) when the defective graphene breaks into two (semi-infinite) graphene nanoribbons, one with a zigzag edge and the other with an armchair-like (pentagon) edge. A large spin polarization is localized on the zigzag edge but none on the armchair-like edge, leading to a large local magnetic moment. Meanwhile, the strain energy also undergoes a sudden change due to the structural breakage and so does the energy difference between the nonmagnetic and ferromagnetic states (Figure 5b).

CONCLUSION

Our first-principles calculations predict a ferromagnetic ground state for graphene with topological line defect with spin-polarized electrons localized within the extended line defect region. The weak magnetism and its stability can be enhanced greatly by strain applied along the zigzag direction but is sharply reduced when the strain is over a critical value. In sharp contrast, tensile strain along the armchair direction reduces the magnetism before structural breakage. A detailed analysis of our calculated results indicates that this strain-induced intriguing magnetic modulation is related to changes in electron correlation and the accompanying redistribution of spin polarization arising from local bond length variation in the line defect region. The tunable magnetism and its stability *via* strain control make such defective graphene a promising candidate for applications in future spintronic nanodevices.

METHODS

Our calculations are performed using the SIESTA package[28] with the local spin density approximation (LSDA) for the exchange correlation function.[29] The double-ζ polarized numerical atomic orbital basis sets for C are used. All atoms are allowed to relax until the force on each atom is less than 0.02 eV/Å. The Brillouin integration is sampled with 10 × 10 × 1 Monkhorst meshes. An equivalent plane wave cutoff of 300 Ry is chosen in the simulations. Vacuum layers of at least 10 Å are chosen in the thickness direction. A representative graphene model with topological line defect is shown in Figure 1a, in which octagons and pentagons are alternatively aligned parallel to the zigzag direction.

Acknowledgment. Work at UNLV is supported by DOE Cooperative Agreement (No. De-FC52-06NA26274). It is also supported by the 973 Program (No. 2007CB936204), National NSF (No. 10732040) of China.

REFERENCES AND NOTES

1. Zhang, Y.; Tan, Y.-W.; Stormer, H. L.; Kim, P. Experimental Observation of the Quantum Hall Effect and Berry's Phase in Graphene. *Nature* **2005,** *438*, 201–204.
2. Blake, P.; Brimicombe, P. D.; Nair, R. R.; Booth, T. J.; Jiang, D.; Schedin, F.; Ponomarenko, L. A.; Morozov, S. V.; Gleeson, H. F.; Hill, E. W.; *et al.* Graphene-Based Liquid Crystal Device. *Nano Lett.* **2008,** *8*, 1704–1708.
3. Kim, W. Y.; Kim, K. S. Prediction of Very Large Values of Magnetoresistance in a Graphene Nanoribbon Device. *Nat. Nanotechnol.* **2008,** *3*, 408–412.
4. Geim, A. K.; Novoselov, K. S. The Rise of Graphene. *Nat. Mater.* **2007,** *6*, 183–191.
5. Geim, A. K. Graphene: Status and Prospects. *Science* **2009,** *324*, 1530–1534.
6. Jung, N.; Kim, N.; Jockusch, S.; Turro, N. J.; Kim, P.; Brus, L. Charge Transfer Chemical Doping of Few Layer

Graphenes: Charge Distribution and Band Gap Formation. *Nano Lett.* **2009,** *9*, 4133–4137.
7. Zhang, Y.; Tang, T.-T.; Girit, C.; Hao, Z.; Martin, M. C.; Zettl, A.; Crommie, M. F.; Shen, Y. R.; Wang, F. Direct Observation of a Widely Tunable Bandgap in Bilayer Graphene. *Nature* **2009,** *459*, 820–823.
8. Castro Neto, A. H.; Guinea, F.; Peres, N. M. R.; Novoselov, K. S.; Geim, A. K. The Electronic Properties of Graphene. *Rev. Mod. Phys.* **2009,** *81*, 109–162.
9. Botello-Méndez, A. R.; Cruz-Silva, E.; López-Urías, F.; Sumpter, B. G.; Meunier, V.; Terrones, M.; Terrones, H. Spin Polarized Conductance in Hybrid Graphene Nanoribbons Using 5−7 Defects. *ACS Nano* **2009,** *3*, 3606–3612.
10. Lusk, M. T.; Carr, L. D. Nanoengineering Defect Structures on Graphene. *Phys. Rev. Lett.* **2008,** *100*, 175503.
11. Hashimoto, A.; Suenaga, K.; Gloter, A.; Urita, K.; Iijima, S. Direct Evidence for Atomic Defects in Graphene Layers. *Nature* **2004,** *430*, 870–873.
12. Han, K. H.; Spemann, D.; Esquinazi, P.; Höhne, R.; Riede, V.; Butz, T. Ferromagnetic Spots in Graphite Produced by Proton Irradiation. *Adv. Mater.* **2003,** *15*, 1719.
13. Vozmediano, M. A. H.; Lopez-Sancho, M. P.; Stauber, T.; Guinea, F. Local Defects and Ferromagnetism in Graphene Layers. *Phys. Rev. B* **2005,** *72*, 155121.
14. Yazyev, O. V.; Helm, L. Defect-Induced Magnetism in Graphene. *Phys. Rev. B* **2007,** *75*, 125408.
15. Yazyev, O. V. Emergence of Magnetism in Graphene Materials and Nanostructures. *Rep. Prog. Phys.* **2010,** *73*, 056501.
16. Wang, Y.; Huang, Y.; Song, Y.; Zhang, X.; Ma, Y.; Liang, J.; Chen, Y. Room-Temperature Ferromagnetism of Graphene. *Nano Lett.* **2009,** *9*, 220.
17. Lahiri, J.; Lin, Y.; Bozkurt, P.; Oleynik, I. I.; Batzill, M. An Extended Defect in Graphene as a Metallic Wire. *Nat. Nanotechnol.* **2010,** *5*, 326–329.
18. Okada, S.; Nakada, K.; Kuwabara, K.; Daigoku, K.; Kawai, T. Ferromagnetic Spin Ordering on CarbonNanotubes with Topological Line Defects. *Phys. Rev. B* **2006,** *74*, 121412(R).
19. Kahaly, M. U.; Singh, S. P.; Waghmare, U. V. Carbon Nanotubes with an Extended Line Defect. *Small* **2008,** *4*, 2209–2213.
20. Yazyev, O. V.; Louie, S. G. Electronic Transport in Polycrystalline Graphene. *Nat. Mater.* **2010,** *9*, 806.
21. Mohr, M.; Papagelis, K.; Maultzsch, J.; Thomsen, C. Two-Dimensional Electronic and Vibrational Band Structure of Uniaxially Strained Graphene from *Ab Initio* Calculations. *Phys. Rev. B* **2009,** *80*, 205410.
22. Choi, S. M.; Jhi, S. H.; Son, Y. W. Effects of Strain on Electronic Properties of Graphene. *Phys. Rev. B* **2010,** *81*, 081407.
23. Pereira, V. M.; Castro Neto, A. H.; Peres, N. M. R. Tight-Binding Approach to Uniaxial Strain in Graphene. *Phys. Rev. B* **2009,** *80*, 045401.
24. Viana-Gomes, J.; Pereira, V. M.; Peres, N. M. R. Magnetism in Strained Graphene Dots. *Phys. Rev. B* **2009,** *80*, 245436.
25. Fujita, M.; Wakabayashi, K.; Nakada, K. Peculiar Localized-State at Zigzag Graphite Edge. *J. Phys. Soc. Jpn.* **1996,** *65*, 1920–1923.
26. Topsakal, M.; Ciraci, S. Elastic and Plastic Deformation of Graphene, Silicene, and Boron Nitride Honeycomb Nanoribbons under Uniaxial Tension: A First-Principles Density-Functional Theory Study. *Phys. Rev. B* **2010,** *81*, 024107.
27. Lu, Y.; Guo, J. Band Gap of Strained Graphene Nanoribbons. *Nano Res.* **2010,** *3*, 189–199.
28. Soler, J. M.; Artacho, E.; Gale, J. D.; García, A.; Junquera, J.; Ordejón, P.; Sánchez-Portal, D. The SIESTA Method for *Ab Initio* Order-N Materials Simulation. *J. Phys.: Condens. Matter* **2002,** *14*, 2745–2779.
29. Ceperley, D. M.; Alder, B. J. Ground State of the Electron Gas by a Stochastic Method. *Phys. Rev. Lett.* **1980,** *45*, 566.